Atomistic Insight into Adsorption, Mobility, and Vibration of Water in Ion-Exchanged Zeolite-like Metal−Organic Frameworks

A. Nalaparaju, R. Babarao, X. S. Zhao, and J. W. Jiang*

Department of Chemical and Biomolecular Engineering, National University of Singapore, Singapore 117576

ABSTRACT The adsorption, mobility, and vibration of water in ion-exchanged rho-zeolite-like metal−organic frameworks (ZMOFs) are investigated using atomistic simulations. Because of the high affinity for the ionic framework and nonframework ions, water is strongly adsorbed in rho-ZMOFs with a three-step adsorption mechanism. At low pressures, water is preferentially adsorbed onto Na^+ ions, particularly at site II; with increasing pressure, adsorption occurs near the framework and finally in the large cage. Upon water adsorption, Na^+ ions are observed to redistribute from site I to site II and gradually hydrated with increasing pressure. In Li-, Na-, and Cs-exchanged rho-ZMOFs, the adsorption capacity and isosteric heat decrease with increasing ionic radius attributed to the reduced electrostatic interaction and free volume. The mobility of water in Na-rho-ZMOF increases at low pressures but decreases upon approaching saturation. With sufficient amount of water present, the mobility of Na^+ ions is promoted. The vibrational spectra of water in Na-rho-ZMOF exhibit distinct bands for librational motion, bending, and stretching. The librational motion has a frequency higher than bulk water due to confinement. With increasing loading and hence stronger coordinative attraction, the bending frequency shows a blue shift. Symmetric and asymmetric modes are observed in the stretching as a consequence of the strong water−ion interaction. This study provides a fundamental microscopic insight into the static and dynamic properties of water in charged ZMOFs and reveals the subtle interplay between water and nonframework ions.

KEYWORDS: water · adsorption · mobility · vibration · atomistic simulation · metal−organic frameworks

Water exists ubiquitously in many natural and synthesized nanoporous materials such as zeolites, clays, and proteins.[1,2] As attributed to the surface interactions and geometry constrains, water in nanoconfined space behaves significantly different from bulk water. For instance, unique two-dimensional layers, cyclic pentamers, infinite chains, and helical heptamers were observed for water upon confinement in various nanoporous materials.[3−6] The chemical composition of materials, charged species, and hydration level all come into play in a complicated way and govern the microscopic properties of water. Therefore, an atomic-level understanding of water in nanoporous materials is fundamentally important for tuning material structures, functionalities, and applications.

A large number of experimental and simulation studies have been reported for water in a variety of nanoporous materials including carbons, zeolites, and protein crystals. Gubbins and co-workers examined the structure and melting of water in carbon nanotubes and silica glasses and found that the melting point was depressed relative to bulk water.[7,8] Murad and co-workers suggested that carbon nanotubes could be used for the separation of water and ions from salt solutions.[9,10] Do and co-workers simulated the effects of curvature and surface heterogeneity on water adsorption in finite-length carbon nanopores and proposed a new adsorption−desorption model for water in activated carbon.[11,12] Sholl and co-workers examined the transport properties of hydrogen-bonding liquids (water and alcohols) in single-walled metal−oxide nanotubes and concluded that the hydrogen-bond network of water causes its diffusion behavior different from alcohols.[13] Beauvais *et al.* quantitatively showed the redistribution of nonframework ions in FAU-zeolite during water adsorption, as well as the influence of hydration on the separation of *p*- and *m*-xylene.[14] Di Lella *et al.* studied the effect of preadsorbed water on cation rearrangement and adsorption of hydrocarbon mixtures in zeolites.[15] Demontis *et al.* provided an atomic-scale description on nanoclustered water, along with the intra- and intermolecular vibrational properties of water in zeolites.[16] Nalaparaju *et al.* simulated the adsorption and diffusion of water in Na-exchanged ETS-10 and observed a redistribution of Na^+ ions upon water adsorpiton.[17] Hu and Jiang investigated the spatial and temporal properties

*Address correspondence to chejj@nus.edu.sg.

Received for review June 9, 2009 and accepted August 17, 2009.

Published online August 26, 2009.
10.1021/nn900605u CCC: $40.75

of water in biozeolites—protein crystals with different morphologies and chemical topologies—and found that the flexibility of the protein framework promotes water mobility.[18,19]

In the past decade, there has been explosive interest in applying emerging metal−organic frameworks (MOFs) in a wide variety of applications, such as gas storage and separation, catalysis, and ion exchange.[20−24] MOFs possess well-defined pores with record-breaking surface areas and pore volumes. In many MOFs, water could exist in the samples after synthesis. It was observed that Zn- or Cu-based MOFs are sensitive to moisture and even degrade upon exposure to air.[25] As a consequence, water plays a crucial role in governing their structures and properties. Greathouse and Allendorf found that MOF-5 is stable at very low water content but unstable upon exposure to ≥4% water. They attributed the dissociation of MOF-5 to the weak metal−linker interactions.[26] Kanoh and co-workers experimentally determined water adsorption in pillared-layer MOFs with one-dimensional semirectangular pores and observed type I isotherms.[27] Henninger *et al.* demonstrated that dehydratable−hydratable water-stable MOF could be used for low-temperature heating and cooling.[28] Castillo *et al.* performed a simulation study to understand water adsorption in Cu-BTC and showed that water has a larger affinity for metal sites than light gases and hydrocarbons.[29] Küsgens *et al.* measured water adsorption in Cu-BTC, ZIF-8, MIL-101, and DUT-4 and estimated the hydrophobicity and stability of MOFs toward moisture.[30]

Eddaoudi and co-workers developed a unique subset of MOFs, zeolite-like MOFs (ZMOFs), by utilizing metal centers as nodes and polyatomic organic ligands as linkers.[31−33] ZMOFs are topologically relevant to inorganic zeolites and exhibit similar structural properties. However, the substitution of oxygen atoms in zeolites with tunable organic linkers leads to extra large pores. The edge expansion offers a great potential toward the design and synthesis of very open ZMOFs. Particularly interesting, a number of ZMOFs consist of ionic frameworks with charge-balancing nonframework ions (*e.g.*, rho-ZMOF synthesized by assembly of tetrahedral building units with a long ditopic organic linker).[31] The presence of nonframework ions in charged ZMOFs offers several advantages over neutral structures in many industrial applications. Similar to highly stable zeolites, most ZMOFs largely maintain their structural integrity in water and organic solvents. From a practical point of view, ZMOFs could be potentially used in aqueous media for pervaporation, water treatment, and ion exchange. Therefore, a clear fundamental understanding on the microscopic properties of water in ZMOFs will be a major step forward for their emerging applications. However, currently there is no study reported for water in ZMOF.

Recently, we characterized the extraframework ions and examined the selective adsorption of gas mixtures in dehydrated Na-rho-ZMOF.[34] In this work, we investigate the adsorption, mobility, and vibration of water in ion-exchanged rho-ZMOFs. In Results and Discussion, first we show the locations and dynamics of Na^+ cations in dry Na-rho-ZMOF; then the adsorption sites, isotherms, and isosteric heats are presented for water in rho-ZMOFs; the effect of ion type on water adsorption is also explored. Finally, the mobility and vibration properties of water are reported. In Models and Methods, the models of rho-ZMOFs, ions, and water are described briefly, along with the simulation methods. Specifically, canonical ensemble Monte Carlo simulations were used to identify the locations of Na^+ ions, grand canonical Monte Carlo simulations to predict the adsorption of water, and molecular dynamics simulations to examine the dynamics of Na^+ ions, mobility, and vibration of water.

RESULTS AND DISCUSSION

First, the locations and dynamics of Na^+ ions are characterized in dehydrated Na-rho-ZMOF. Then, the density contours and structural properties are presented for water adsorption in Na-rho-ZMOF, as well as the adsorption isotherms and isosteric heats in rho-ZMOFs with different types of ions. Finally, the mobility of water is examined in Na-rho-ZMOF; the vibrational spectra of water are shown to investigate how vibration is affected by confinement and interplayed with ions.

Locations and Dynamics of Na^+ Ions. The extraframework Na^+ ions in Na-rho-ZMOF have been characterized in our previous study[34] and are briefly described here. Figure 1 shows two types of favorable sites for Na^+ ions. Site I is at the single eight-membered ring (S8MR) and near the entrance to the truncated cuboctahedron (α-cage). Two S8MRs in neighboring unit cells form a double eight-membered ring (D8MR). The distance from site I to the nearest In atoms in S8MR is 5.0−5.3 Å and approximately 7.8 Å to the next-to-nearest In atoms in the D8MR. Site II is in the α-cage and proximal to the four-membered ring (4MR). In one unit cell, 26 Na^+ ions are located at site I and the remaining at site II. The distribution of nonframework ions in the two sites is governed by the attractions between ions and framework, in addition to the repulsions between ions. Compared to site II, site I has a larger coordination number with neighboring atoms in the octagonal S8MR and hence a stronger interaction with the framework. The sites identified here match fairly well with those of Mg^{2+} ions in rho-ZMOF.[33] Nevertheless, a slight difference is observed between monovalent Na^+ and divalent Mg^{2+}. To compensate the framework charges, Mg^{2+} ions are located in less anchored positions in the framework and thus near the center of 4MR in the α-cage. In contrast, the number density of Na^+ ions is doubled, and they an-

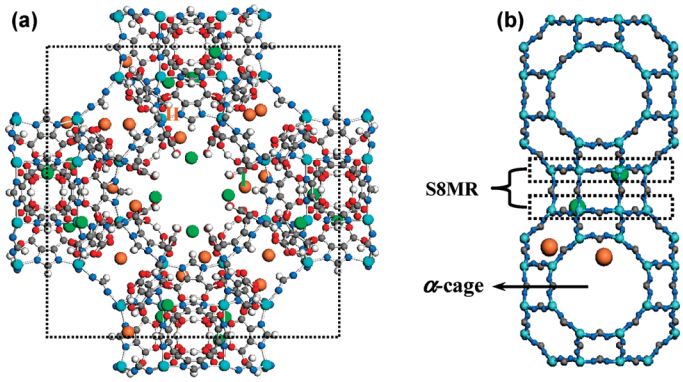

Figure 1. Locations of Na^+ ions in Na-rho-ZMOF. Site I (green) is at the single eight-membered ring (S8MR), while site II (orange) is in the α-cage. (a) Unit cell and (b) eight-membered ring and α-cage. Color code: In, cyan; N, blue; C, gray; O, red; and H, white.

chor closer to the framework. Interestingly, the two types of binding sites in rho-ZMOF resemble those in its inorganic counterpart rho-zeolite.[35] In the latter, however, an additional type of site is located at the center of the D8MR and equally distanced from both S8MRs.

A movie generated from MD simulation is provided in the Supporting Information for the dynamics of Na^+ ions in dehydrated Na-rho-ZMOF. The mobility of Na^+ at site II is greater than at site I due to the relatively weaker interaction with framework and the larger void space available around site II. However, the overall mobility of Na^+ ions in rho-ZMOF is generally small. This is attributed to the strong electrostatic interactions between ions and framework and the degenerated favorable sites away from each other, which largely prohibits ion hopping within the nanosecond time scale of the MD simulation. In addition, the steric hindrance of metal atoms connecting organic linkers also reduces ion mobility.

Adsorption of Water. Figure 2 shows the density contours of adsorbed water in Na-rho-ZMOF at 10^{-8}, 10^{-2}, and 1 kPa. At 10^{-8} kPa, water molecules are localized close to Na^+ ions and scattered from one other. Therefore, the nonframework ions can be regarded as preferential adsorption sites for water.

With increasing pressure to 10^{-2} kPa, water adsorption occurs primarily near the framework surface. At 1 kPa approaching saturation, the large cage is gradually filled and Na^+ ions appear to be solvated by continuously distributed water shells. Such a three-step adsorption mechanism was previously observed for water adsorption in NaX and NaY zeolites.[36] From low to high pressure, the locations of Na^+ ions are observed to shift from site I to II upon water adsorption. It is also found that water adsorbs preferentially near Na^+ ions at site II rather than at site I. This is attributed primarily to the steric effect, as shown in Figure 1, the void space near site II in the α-cage is larger than at site I.

Figure 3a,b shows the radial distribution functions $g(r)$ between Na^+ ions and oxygen atoms (OW) of water, calculated from

$$g_{ij}(r) = \frac{\langle \Delta N_{ij}(r, r + \Delta r) \rangle V}{4\pi r^2 \Delta r N_i N_j} \quad (1)$$

where r is the distance between species i and j, $\langle \Delta N_{ij}(r,r + \Delta r) \rangle$ is the ensemble averaged number of j around i within a shell from r to $r + \Delta r$, V is the system volume, N_i and N_j are the numbers of i and j. For both Na_I^+-OW and Na_{II}^+-OW, a pronounced peak is observed in $g(r)$ at $r = 2.3$ Å, and the peak height drops with increasing pressure. This is due to two factors: first, water molecules are located further away from ions; second, the average density of adsorbed water increases. As we shall see below, however, there are more water molecules around Na^+ ions as water pressure increases; that is, Na^+ ions are solvated by more water molecules. At a given pressure, the peak height is larger in Na_{II}^+-OW than in Na_I^+-OW. This confirms that water is located predominantly near site II. Because of the increasingly cooperative attractions of adsorbed water at site II, Na^+ ions at site I are progressively shifted to site II as pressure increases. Such a redistribution of Na^+ ions

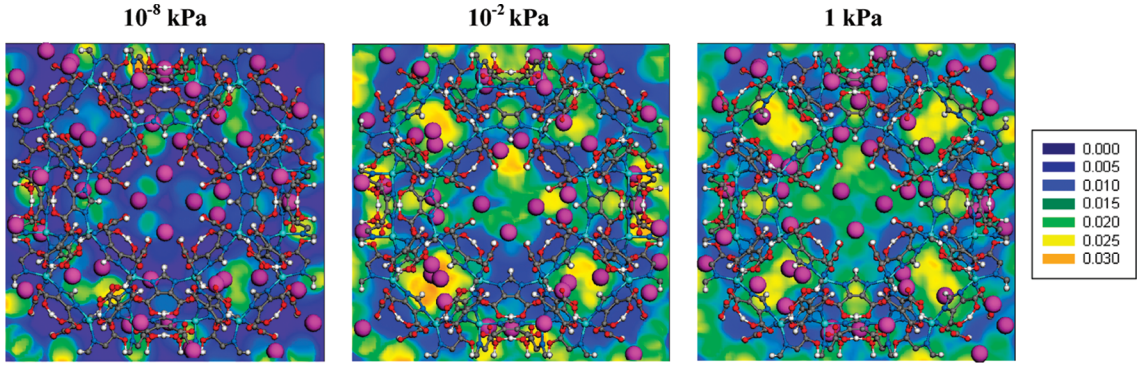

Figure 2. Density contours of water in Na-rho-ZMOF at 10^{-8}, 10^{-2}, and 1 kPa. Na^+ ions are represented by the large pink spheres. The density is based on the number of water molecules per Å^3.

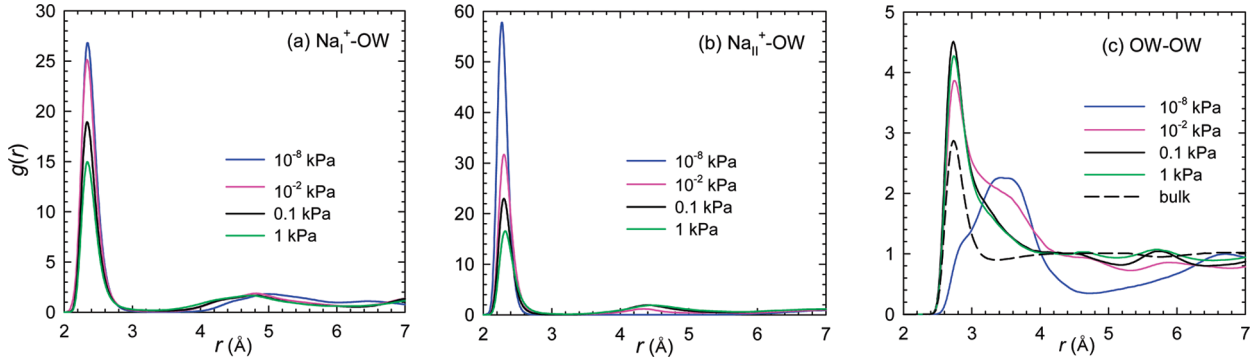

Figure 3. Radial distribution functions of (a) Na_I^+-OW, (b) Na_{II}^+-OW, (c) OW-OW in Na-rho-ZMOF at 10^{-8}, 10^{-2}, 0.1, and 1 kPa. For comparison, $g(r)$ of OW-OW in bulk water is included as the dashed line in (c).

is observed in Figure 2 and will be discussed further below. The second peak in $g(r)$ of Na-OW is indistinct, unlike the case of water adsorption in NaX and NaY.[36] This is because rho-ZMOF has a very open structure with extra large cavity. Figure 3c shows $g(r)$ of OW-OW for water adsorption in Na-rho-ZMOF and for bulk water. At 10^{-8} kPa, the peak of $g(r)$ in Na-rho-ZMOF is located at 3.3−3.6 Å, and this relatively long distance is between the scattered water molecules near the neighboring Na^+ ions, as seen in Figure 2. With increasing pressure, water molecules get closer, form a hydration shell, and behave as bulk water. Consequently, $g(r)$ of OW-OW exhibits a peak at 2.7 Å resembling bulk water. In the literature, it was observed that the peak location of water in ionic solutions is similar to bulk water.[37]

Figure 4 shows the coordination numbers of water N_{water} around Na^+ ions as a function of distance r between ion and water. N_{water} was calculated from

$$N_{water}(r) = \rho_{water} \int_0^r g_{Na^+-water}(r')4\pi r'^2 dr' \qquad (2)$$

where ρ_{water} is the average density of water. As seen earlier in Figure 3, the peak height of g(r) for both Na_I^+-OW and Na_{II}^+-OW drops with increasing pressure. Nevertheless, N_{water} becomes larger with pressure at any given r. This simply reveals that the number of water molecules around Na^+ ions increases as pressure increases. In other words, Na^+ ions are hydrated in a greater degree. At r = 3.4 Å, corresponding to the first minimum of $g(r)$ in Figure 3a,b, N_{water} of Na_{II}^+ is larger than that of Na_I^+, especially at 10^{-8} kPa. This further demonstrates the preferential location of water near Na^+ ions at site II rather than site I.

The adsorption isotherms of water in Li-, Na-, and Cs-exchanged rho-ZMOFs are shown in Figure 5, as well as in Figure S3 in the Supporting Information at low-pressure regime. At low pressures, adsorption increases sharply, indicating a micropore-filling mechanism. This is attributed to the strong affinity of water for the ionic framework and the nonframework ions. With increasing pressure, adsorption tends to approach saturation. The isotherms in all three systems exhibit the same shape and belong to type I as classified by IUPAC. Nevertheless, the extent of adsorption is the largest in Li-rho-ZMOF, followed by Na-rho-ZMOF and Cs-rho-ZMOF. In other words, adsorption becomes weak with increasing size of alkali ion in rho-ZMOFs. The porosity is estimated to be 0.55, 0.54, and 0.50 in Li-, Na-, and Cs-exchanged rho-ZMOFs, respectively. A smaller ion interacts with water more strongly due to greater local electric fields around the ion. With increasing ionic size, the interaction between ion and water is reduced, in addition to the free volume. These results are in good accordance with water adsorption in cation-exchanged FAU zeolite.[38]

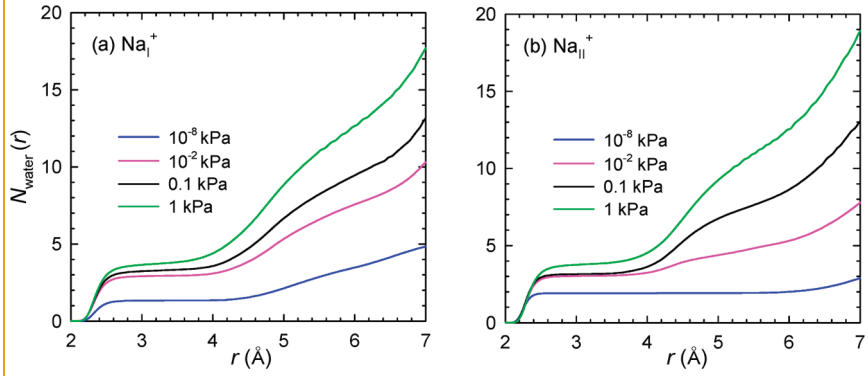

Figure 4. Coordination numbers of water around (a) Na_I^+ and (b) Na_{II}^+ in Na-rho-ZMOF at 10^{-8}, 10^{-2}, 0.1, and 1 kPa.

The inset of Figure 5 quantitatively shows the numbers of Na^+ ions at sites I and II as a function of loading. As loading increases, Na_I^+ ions decrease from 26 to 22 and, correspondingly, Na_{II}^+ ions increase from 22 to 26. As discussed above, the redistribution of Na^+ ions from site I to II is due to the preferential adsorption of water near Na_{II}^+ ions, which in turn exerts attractive force on Na_I^+ ions and facilitates them to relocate. In our recent study, the redistribution of Na^+ ions in Na-ETS-10 was also observed upon water adsorption.[17]

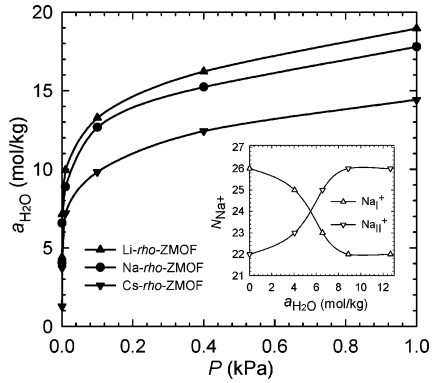

Figure 5. Calculated adsorption isotherms of water in Li-, Na-, and Cs-exchanged rho-ZMOFs as a function of pressure. The inset shows the numbers of Na_I^+ and Na_{II}^+ as a function of water loading in Na-rho-ZMOF.

The isosteric heat of water adsorption was calculated from

$$Q_{st} = RT - \left[\frac{\partial(U_{total} - U_{intra})}{\partial a}\right]_{T,V} \quad (3)$$

where R is gas constant, a is loading of water, U_{total} is the total adsorption energy including contributions from both adsorbate−adsorbent and adsorbate−adsorbate interactions, and U_{intra} is the intramolecular energy of water. Compared with adsorption isotherm, isosteric heat is more sensitive to loading thus more commonly used to ascertain the adsorption mechanism. Figure 6 shows Q_{st} of water in Li-, Na-, and Cs-exchanged rho-ZMOFs as a function of loading. At infinite dilution, Q_{st} is about 156.4, 131.5, and 104.1 kJ/mol in Li-, Na-, and Cs-rho-ZMOFs, respectively. At any given loading, Q_{st} in Cs-rho-MOF is consistently smaller than in Li- and Na-rho-ZMOFs. As discussed earlier, this is because the electrostatic interaction of water with a larger cation is weaker. The decrease in isosteric heat with increasing size of cation was previously observed in cation-exchanged zeolites.[38] In all-silica MFI and BEA, Q_{st} is in the range of 80−50 kJ/mol, significantly lower than in the proton-exchanged counterparts.[39] This reveals that the framework charges and nonframework ions play a crucial role in water adsorption. In all of the three systems, Q_{st} drops as loading rises, indicating the energetic heterogeneity of the framework. With a closer look, we can find three regions with different slopes, particularly in Li-rho-ZMOF: 0−5, 5−15, and beyond 15 mol/kg. This corresponds to the three-step adsorption observed in Figure 2. Water is initially adsorbed onto the nonframework ions, then close to the framework surface, and finally in the large cage. Near saturation, Q_{st} approaches a value of 40−50 kJ/mol, which is approximately the enthalpy of vaporization of bulk water.

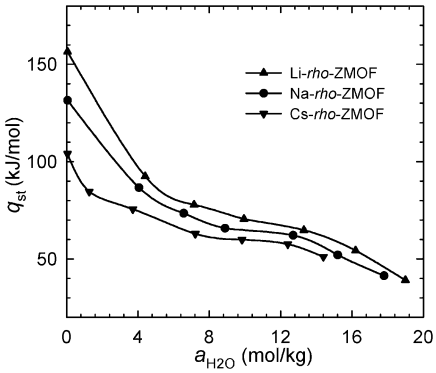

Figure 6. Calculated isosteric heats of water adsorption in Li-, Na-, and Cs-exchanged rho-ZMOFs as a function of loading.

Figure 7 shows the locations of water in Li-, Na-, and Cs-exchanged rho-ZMOFs at a bulk pressure of 10^{-8} kPa. For clarity, only water molecules in the S8MR are shown. The adsorbed water molecules interact with the nonframework ions and carbonyl groups. The distance between water and ion is approximately 2.1−2.3 Å in Li-rho-ZMOF, 2.3−2.5 Å in Na-rho-ZMOF, and 3.1−3.7 Å in Cs-rho-ZMOF. The distance increasing from Li-, Na-, to Cs-rho-ZMOF is attributed to the reduced electrostatic interaction for a larger cation, as discussed earlier. This trend was also observed for CO_2 adsorption in ion-exchanged FAU zeolites.[40] Due to the formation of H bonds, interestingly, water molecules in all the three rho-ZMOFs are oriented in such a way that the hydrogen atoms point toward the carbonyl groups.

Mobility of Water. The mobility of water was analyzed by mean-squared displacement (MSD) from MD simulation

$$\mathrm{MSD}(t) = \frac{1}{KN}\sum_{k}^{K}\sum_{i=1}^{N}|\mathbf{r}_i(t + t_k) - \mathbf{r}_i(t_k)|^2 \quad (4)$$

where t is time, N is the number of water molecules, and $\mathbf{r}_i(t)$ is the position of ith water at time t. The multiple time-origin method was used to evaluate MSDs, and K is the number of time origins. Figure 8 shows the MSDs of water in Na-rho-ZMOF at various pressures. At low pressures, water is strongly adsorbed onto the nonframework ions. Thus, water exhibits a local motion around ions with a negligible mobility. With increasing pressure, ions are gradually solvated by hydration shells and water experiences less interaction with ions; consequently, water can move relatively free in the large cavity, and the mobility increases. Near saturation, however, steric hindrance plays a dominant role; that is, there is no large room available for motion, and hence, the mobility is retarded. In principle, if all of the empty space is filled, molecules cannot hop from one place to other and mobility becomes essentially zero. The trend is similar to the behavior of water in Na-ETS-10[17] and FAU zeolite.[36]

The dynamics of nonframework Na^+ ions can be substantially affected by adsorbed water. In the Supporting Information, movies are shown for Na^+ ions in Na-rho-ZMOF at different water loadings (with 360, 486,

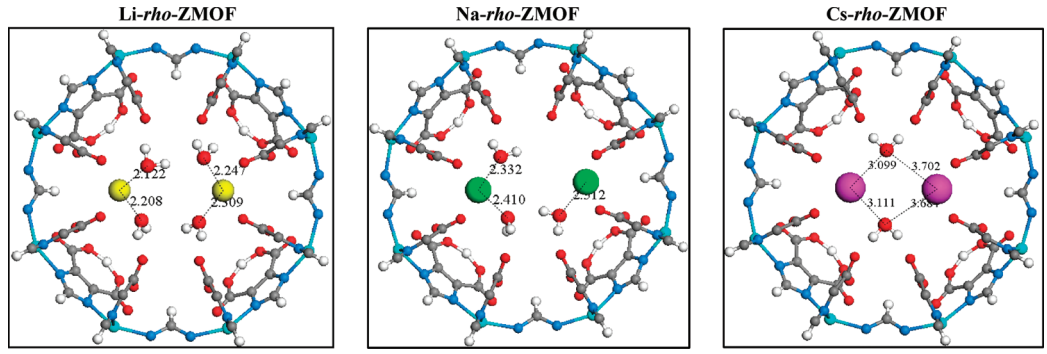

Figure 7. Locations of water in the single eight-membered ring in Li-, Na-, and Cs-exchanged rho-ZMOFs at 10^{-8} kPa. Color code: In, cyan; N, blue; C, gray; O, red; H, white; Li^+, yellow; Na^+, green; and Cs^+, pink. The distances between water and ions are in angstroms.

and 531 water molecules in one unit cell). Like in dehydrated Na-rho-ZMOF, the mobility of Na^+ ions is marginal at a loading less than 486. Interestingly, several Na^+ ions are found to move rather fast at loading of 486 or 531, implying that the dynamics of ions can be enhanced in the presence of sufficient amount of water. This is attributed to the strong interactions of water with the ionic framework and nonframework ions, which substantially perturbs ion distribution and promotes ion migration.

Vibration of Water. Spectroscopy is commonly used to probe the structure and dynamics of fluids. The peak position, bandwidth, and intensity of spectra in confined space are different from those in bulk phase and extremely sensitive to the changes of geometry and strength upon confining. To obtain the vibrational information of water adsorption in Na-rho-ZMOF, the normalized velocity autocorrelation functions (VACFs) $C_v(t)$ were estimated from MD simulation

$$C_v(t) = \frac{\langle u(0) \cdot u(t) \rangle}{\langle u(0) \cdot u(0) \rangle} \quad (5)$$

where $u(t)$ is the velocity of hydrogen atoms of water at time t. The spectra were then calculated by the Fourier transform of VACFs

$$I(v) = \int_0^{+\infty} C_v(t) \cos(vt) dt \quad (6)$$

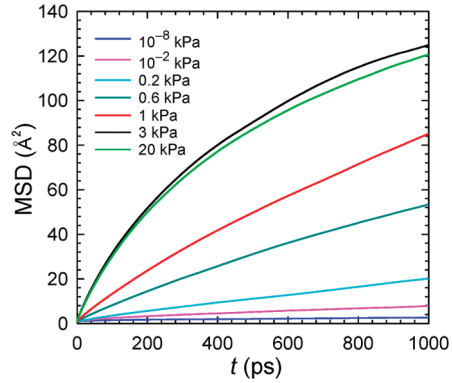

Figure 8. Mean-squared displacements of water in Na-rho-ZMOF at various pressures.

where v is wavenumber. The fast Fourier transform technique was used for this calculation.

Figure 9 shows the simulated vibrational spectra of water in Na-rho-ZMOF at various pressures. For comparison, the spectra of bulk water were also calculated and found to be consistent with the literature results.[41] Three distinct bands are observed for water in Na-rho-ZMOF, corresponding to the librational motion, H−O−H bending, and H−O stretching of water, respectively. The frequency of librational motion in rho-ZMOF (~500 cm^{-1}) is, due to confinement, higher than in bulk water (~420 cm^{-1}). As pressure increases, the confinement effect is enhanced and a blue shift is observed in the peak. A similar effect was observed for the librational motion of water in FER zeolite.[42] For H−O−H bending, the frequency in rho-ZMOF is around 1440 cm^{-1}, slightly lower than in bulk water (~1450 cm^{-1}). With increasing pressure, however, the bending frequency exhibits a blue shift and is closer to bulk water. This is because of the increasing coordination with the increased number of surrounding water molecules.[43] Consequently, the behavior of confined water gradually approaches bulk water, and the number of H bonds increases. The two pronounced frequencies around 3670 and 3720 cm^{-1} are identified to be the symmetric and asymmetric modes of H−O stretching. The splitting of symmetric and asymmetric modes, occurring particularly at low loadings, is similar to the behavior of interfacial water.[44] This is attributed to the strong interactions between water and cations, which break the regular tetrahedral arrangement of water and lead to a decrease in the number of H bonds. As loading increases, the coordination with the surrounding water molecules becomes stronger and the stretching band has a red shift and is close to bulk water.

Among the three vibrational modes, the H−O stretching is very sensitive to the change in the connectivity degree of the H-bond network in the surrounding water, while the librational motion and H−O−H bending depends largely on the local arrangement of water molecules.[45] In a porous material with structure-making capability, the confined water behaves close to

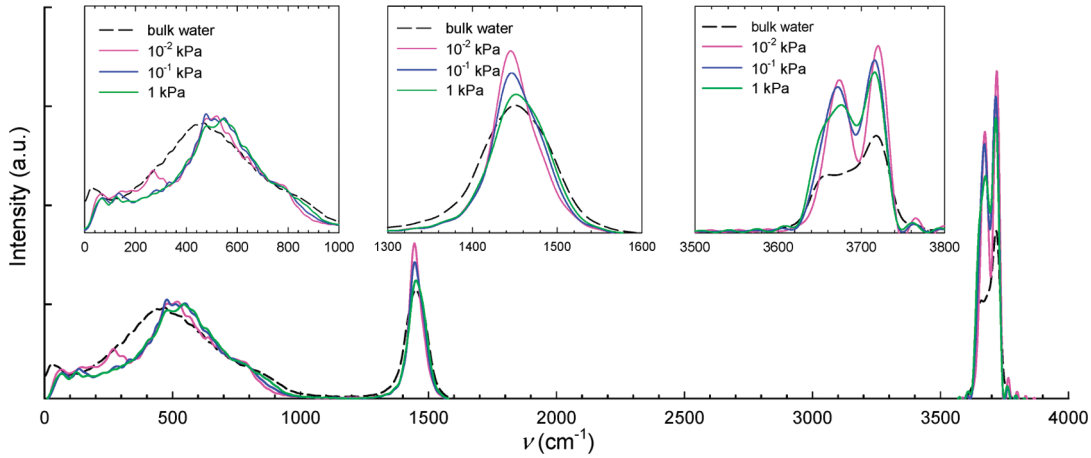

Figure 9. Vibrational spectra of water in Na-rho-ZMOF at various pressures and in bulk water.

bulk water; consequently, the librational motion and H−O−H bending are generally similar to bulk water. For all of the three bands in Na-rho-ZMOF, the spectral intensity and width exhibit a similar trend as a function of pressure. At low pressures, the intensity is large because water is adsorbed onto cations and scattered, thus the distance of the H bond is long, the vibration has great amplitude, and the width is narrow due to the limited number of H bonds. At high pressure, water molecules stay close to one another and the number of H-bonds increases; consequently, the spectra have small amplitude and wide bandwidth.

CONCLUSIONS

We have investigated the adsorption, mobility, and vibration of water in ion-exchanged rho-ZMOFs using atomistic simulations. As a 4-connected ZMOF with topology similar to rho-zeolite, rho-ZMOF is a very open framework with an extra large cavity. It contains a large number of charge-balancing cations to neutralize the anionic framework. Two types of favorable sites were identified for Na^+ ions in dehydrated Na-rho-ZMOF. Site I is at the single eight-membered ring, and site II is in the α-cage. Ions at site I have a larger coordination number with the neighboring atoms and hence stronger interaction with the framework. The locations of Na^+ ions identified are in accord with Mg^{2+} ions and resemble those in rho-zeolite. The mobility of ions in dehydrated rho-ZMOF is generally small.

Attributed to the high affinity of water for the ionic framework and the nonframework ions, water is strongly adsorbed in rho-ZMOFs with a three-step adsorption mechanism. At low pressures, water is adsorbed proximally to Na^+ ions. With increasing pressure, adsorption occurs near the framework and finally in the large cage. Interestingly, water is adsorbed preferentially near Na^+ ions at site II; Na^+ ions at site I are progressively shifted to site II upon water adsorption. With increasing pressure, water molecules get closer, form hydration shells around ions, and behave largely like bulk water. For different ions (Li^+, Na^+, and Cs^+), the interaction between ion and water is reduced with increasing ionic size. Consequently, the extent of adsorption and isosteric heat decreases following the order of Li-rho-ZMOF, Na-rho-ZMOF, and Cs-rho-ZMOF.

Water exhibits a negligible local motion around ions at low pressures. Nevertheless, the mobility increases with pressure and finally decreases upon saturation. The mobility of Na^+ ions is enhanced at sufficiently high loadings of water. Three distinct spectral bands were observed for water in Na-rho-ZMOF, corresponding to the librational motion, bending, and stretching of water, respectively. The frequency of librational motion is blue-shifted from that of bulk water, attributed to confinement effect. With increasing pressure, the bending exhibits a blue shift because of the increasing coordinative attraction of water. The stretching splits into symmetric and asymmetric modes at low pressures due to the strong water−cation interaction and approaches the band of bulk water as pressure increases. For the three bands of water vibration in Na-rho-ZMOF, the spectral amplitude drops and the width broadens with increasing pressure.

MODELS AND METHODS

Water was represented by the flexible three-point transferable interaction potential model (TIP3P/Fs).[46] The heat of vaporization predicted by the TIP3P/Fs model is 43.68 kJ/mol, very close to experimental value of 43.93 kJ/mol. This model also satisfactorily reproduces the essential aspects of water vibration. The intramolecular interaction, u^{intra}, in TIP3P/Fs includes harmonic bond-stretching and bond-bending potentials

$$u^{intra} = \frac{k_b}{2}[(r_{OH_1} - r^{\circ}_{OH})^2 + (r_{OH_2} - r^{\circ}_{OH})^2] + \frac{k_\theta}{2}(\theta_{\angle HOH} - \theta^{\circ}_{\angle HOH})^2 \quad (7)$$

where force constant k_b = 4427.297 kJ/mol/Å^2 and equilibrium bond length r°_{OH} = 0.96 Å; force constant k_θ = 284.604 kJ/mol/rad^2 and equilibrium bond angle $\theta^{\circ}_{\angle HOH}$ = 104.5°. The intermo-

lecular u^{inter} is a combination of Lennard-Jones (LJ) and Coulombic potentials

$$u^{inter}(r) = \sum_{i,j} 4\varepsilon_{ij}\left[\left(\frac{\sigma_{ij}}{r_{ij}}\right)^{12} - \left(\frac{\sigma_{ij}}{r_{ij}}\right)^{6}\right] + \frac{q_i q_j}{4\pi\varepsilon_0 r_{ij}} \quad (8)$$

where ε_{ij} and σ_{ij} are LJ well depth and collision diameter, q_i is the atomic charge on ith atom, $\varepsilon_0 = 8.8542 \times 10^{-12}$ C^2 N^{-1} m^{-2} is the permittivity of vacuum. Table 1 lists the corresponding LJ parameters and atomic charges.

As the first example of a 4-connected MOF based on the topology of rho-zeolite, rho-ZMOF possesses a space group of *Im*3m and a lattice constant of 31.062 Å. It was synthesized by metal−ligand-directed assembly of In atoms and 4,5-imidazoledicarboxylic acid (H_3ImDC).[31] Each In atom is coordinated to four N atoms and four O atoms of four separate doubly deprotonated H_3ImDC (HImDC) ligands, respectively, to form an eight-coordinated molecular building block, as shown in Figure S1 in the Supporting Information. Each HImDC is coordinated to two In atoms by forming two rigid five-membered rings *via* N,O-heterochelation. The rho-ZMOF has a truncated cuboctahedron (α-cage) containing 48 In atoms, which link together through double eight-membered rings (D8MR). The substitution of oxygen in rho-zeolite with HImDC generates a very open framework with an extra large cavity of 18.2 Å in diameter. Unlike rho-zeolite and other rho-aluminosilicate or aluminophosphate, rho-ZMOF contains twice as many positive charges (48 *vs* 24) in a unit cell to neutralize the anionic framework. On the basis of the charge density (number of charges per cubic nanometer), however, rho-zeolite may contain higher charge density than rho-ZMOF. The as-synthesized negatively charged rho-ZMOF contains charge-balancing doubly protonated 1,3,4,6,7,8-hexahydro-2*H*-pyrimido[1,2-*a*]pyrimidine (HPP). The HPP organic cations in the parent framework are fully exchangeable with other organic and inorganic cations. For instance, Na-exchanged rho-ZMOF with structural formula $[In_{48}(C_5N_2O_4H_2)_{96}][Na^+_{48}(H_2O)_{282}]$ was obtained by replacing HPP cations with Na^+ ions. Experimental thermogravimetric analysis showed that all residential water molecules in Na-rho-ZMOF can be completely evacuated.[31]

The atomic charges of the rho-ZMOF framework were calculated by density functional theory (DFT) on a fragmental cluster shown in Figure S2 in the Supporting Information. It has been commonly recognized that quantum mechanically derived charges fluctuate appreciably with small basis sets. Nevertheless, they tend to converge beyond the basis set 6-31G(d). Consequently, 6-31G(d) was used in our DFT calculations for all atoms except In atoms, for which the LANL2DZ basis set was used. The DFT computations used the Lee−Yang−Parr correlation functional (B3LYP) and were carried out with Gaussian03 package.[47] It is noteworthy that the concept of atomic charges is solely an approximation, and currently, no unique straightforward method is available to determine atomic charges rigorously. In our study, the atomic charges were estimated by fitting to the electrostatic potential (ESP). The nonframework ions considered were alkali Li^+, Na^+, and Cs^+ each with a positive unit charge. The dispersion interactions of framework atoms and ions were represented by LJ potential with parameters from the universal force field (UFF),[48] as listed in Table 1. The Lorentz−Berthelot combining rules were used to estimate the cross LJ parameters between water, ions, and framework atoms. Our recent study showed that UFF can predict water adsorption in Na-exchanged ETS-10 fairly well.[17] A similar force field, DREIDING, was found being applicable for water adsorption in Cu-BTC.[29]

TABLE 1. Potential Parameters for Water Atoms (OW and HW), Ions (Li^+, Na^+, and Cs^+) and Framework Atoms (In, N, O, C, and H)

atom/ion	σ (Å)	ε (kJ/mol)	*q* (*e*)
OW	3.1506	0.6362	−0.834
HW	0	0	+0.417
Li^+	2.184	0.104	+1
Na^+	2.658	0.126	+1
Cs^+	4.024	0.188	+1
In	3.976	2.504	shown in Figure S2
N	3.260	0.288	
O	3.118	0.251	
C	3.431	0.439	
H	2.571	0.184	

The locations of Na^+ ions in dehydrated Na-rho-ZMOF were characterized using Monte Carlo (MC) simulation in canonical ensemble (NVT) at 298 K. The simulation box contained a unit cell of rho-ZMOF with 48 Na^+ ions, and the periodic boundary conditions were applied in three dimensions. The unit cell was divided into three-dimensional grids with the potential energy maps tabulated in advance and then used by interpolation during simulation. In such a way, the simulation was accelerated by 2 orders of magnitude. A spherical cutoff of 15.0 Å was used to evaluate the LJ interactions, and beyond the cutoff, the usual long-range corrections for a homogeneous system were used. For the Coulombic interactions, a simple spherical truncation could result in significant errors; consequently, the Ewald sum with a tinfoil boundary condition was used. The real/reciprocal space partition parameter and the cutoff for reciprocal lattice vectors were chosen to be 0.2 $Å^{-1}$ and 8, respectively, to ensure the convergence of the Ewald sum. The 48 Na^+ ions were introduced into the system randomly and followed by 10^7 trial moves. Two types of trial moves were used with equal probability, including displacement and regrowth. In the former, a randomly chosen Na^+ ion attempted to move around its initial position, while in the latter, the Na^+ ion attempted to grow in a randomly selected position, which could be considered as "jump move" in the entire simulation box.

Grand canonical Monte Carlo (GCMC) simulations were carried out for water adsorption in Li-, Na-, and Cs-exchanged rho-ZMOFs at 298 K. Because the chemical potentials of adsorbate in adsorbed and bulk phases are identical at thermodynamic equilibrium, GCMC simulation allows one to directly relate the chemical potentials of adsorbate in both phases and has been widely used to simulate adsorption. In this study, the bulk phase was vapor water at room temperature and thus behaved approximately as ideal gas. The framework was assumed to be rigid during simulation because adsorption involves low-energy equilibrium configurations, and the framework flexibility has only a marginal effect. The potential energy between framework and each type of adsorbate atom or ion was pretabulated. The LJ interactions and Coulombic interactions were calculated using the same way as in the NVT simulation mentioned above. The number of trial moves in a typical simulation was 2×10^7, though additional trial moves were used at high loadings. The first 10^7 moves were used for equilibration and the subsequent 10^7 moves for ensemble averages. Five types of trial moves were randomly attempted in the GCMC simulation, namely, displacement, rotation, and partial regrowth at a neighboring position; complete regrowth at a new position; and swap with the reservoir including creation and deletion with equal probability. The nonframework ions were allowed to move, and as we shall observe, the locations of ions were indeed altered upon water adsorption.

Molecular dynamics (MD) simulations were performed to examine the dynamics of Na^+ ions in dehydrated Na-rho-ZMOF and the mobility of adsorbed water in wet Na-rho-ZMOF. The Nosé−Hoover thermostat was used to maintain temperature at 298 K. The initial configurations were taken from the above MC simulations. In MD simulations, 1 ns equilibration and 2 ns production were conducted. The potential and kinetic energies were monitored to ensure equilibration. A time step of 1 fs was used to ensure proper energy conservation. Trajectory in production run was saved every 1 ps to calculate the mean-squared displacements (MSDs) of water. In addition, a 20 ps trajectory was saved every 1 fs to calculate the velocity autocorrelation functions of hydrogen atoms in water, which were then used to obtain vibrational spectra. DL_POLY program was used in the MD simulations.[49]

Acknowledgment. This work was supported by the National University of Singapore and the Singapore National Research Foundation.

Supporting Information Available: Molecular building block, atomic charges, adsorption isotherms at low-pressure regime, and movies for the dynamics of nonframework ions in Na-rho-ZMOF (in the absence and presence of water). This material is available free of charge *via* the Internet at http://pubs.acs.org.

REFERENCES AND NOTES

1. Bagchi, B. Water Dynamics in the Hydration Layer around Proteins and Micelles. *Chem. Rev.* **2005**, *105*, 3197–3219.
2. Ball, P. Water as a Biomolecule. *ChemPhysChem* **2008**, *9*, 2677.
3. Janiak, C.; Scharmann, T. G.; Mason, S. A. Two-Dimensional Water and Ice Layers: Neutron Diffraction Studies at 278, 263, and 20 K. *J. Am. Chem. Soc.* **2002**, *124*, 14010–14011.
4. Naskar, J. P.; Drew, M. G. B.; Hulme, A.; Tocher, D. A.; Datta, D. Occurrence of Ribbons of Cyclic Water Pentamers in a Metallo-Organic Framework Formed by Spontaneous Fixation of CO_2. *CrystEngComm* **2005**, *7*, 67–70.
5. Liu, Q. Y.; Xu, L. $(H_2O)_{12}$-Containing Infinite Chain Encapsulated in Supramolecular Open Framework Built of Cadmium(Ii), 1,3-Di(4-pyridyl)propane and 5-Sulfoisophthalic Acid Monosodium Salt. *CrystEngComm* **2005**, *7*, 87–89.
6. Hedayetullah Mir, M.; Wang, L.; Wong, M. W.; Vittal, J. J. Water Helicate $(H_2O)_7$ Hosted by a Diamondoid Metal−Organic Framework. *Chem. Commun.* **2009**, 4539–4541.
7. Radhakrishnan, R.; Gubbins, K. E.; Sliwinska-Bartkowiak, M. Melting Behavior of Water in Cylindrical Pores. *J. Chem. Phys.* **2002**, *116*, 1147.
8. Sliwinska-Bartkowiak, M.; Jazdzewska, M.; Huang, L. L.; Gubbins, K. E. Melting Behavior of Water in Cylindrical Pores: Carbon Nanotubes and Silica Glasses. *Phys. Chem. Chem. Phys.* **2008**, *10*, 4909.
9. Liu, H. M.; Murad, S.; Jameson, C. J. Ion Permeation Dynamics in Carbon Nanotubes. *J. Chem. Phys.* **2006**, *125*, 084713.
10. Banerjee, S.; Murad, S.; Puri, I. K. Preferential Ion and Water Intake Using Charged Carbon Nanotubes. *Chem. Phys. Lett.* **2007**, *434*, 292–296.
11. Do, D. D.; Junpirom, S.; Do, H. D. A New Adsorption−Desorption Model for Water Adsorption in Activated Carbon. *Carbon* **2009**, *47*, 1466–1473.
12. Wongkoblap, A.; Do, D. D. Adsorption of Water in Finite Length Carbon Slit Pore: Comparison between Computer Simulation and Experiment. *J. Phys. Chem. B* **2007**, *111*, 13949–13956.
13. Zang, J.; Konduri, S.; Nair, S.; Sholl, D. S. Self-Diffusion of Water and Simple Alcohols in Single-Walled Aluminosilicate Nanotubes. *ACS Nano* **2009**, *3*, 1548–1556.
14. Beauvais, C.; Boutin, A.; Fuchs, A. H. A Numerical Evidence for Cation Redistribution upon Water Adsorption. *ChemPhysChem* **2004**, *5*, 1791.
15. Di Lella, A.; Desbiens, N.; Boutin, A.; Demachy, I.; Ungerer, P.; Bellat, J. P.; Fuchs, A. H. Molecular Simulation Studies of Water Physisorption in Zeolites. *Phys. Chem. Chem. Phys.* **2006**, *8*, 5396–5406.
16. Demontis, P.; Gulin-Gonzalez, J.; Jobic, H.; Masia, M.; Sale, R.; Suffritti, G. B. Dynamical Properties of Confined Water Nanoclusters: Simulation Study of Hydrated Zeolite NaA: Structural and Vibrational Properties. *ACS Nano* **2008**, *2*, 1603–1614.
17. Nalaparaju, A.; Zhao, X. S.; Jiang, J. W. Molecular Interplay of Cations and Nonpolar/Polar Sorbates in Titanosilicate ETS-10. *J. Phys. Chem. C* **2008**, *112*, 12861–12868.
18. Hu, Z. Q.; Jiang, J. W. Molecular Dynamics Simulations for Water and Ions in Protein Crystals. *Langmuir* **2008**, *24*, 4215–4223.
19. Hu, Z. Q.; Jiang, J. W. Electrophoresis in Protein Crystal: Nonequilibrium Molecular Dynamics Simulations. *Biophys. J.* **2008**, *95*, 4148–4156.
20. Eddaoudi, M.; Kim, J.; Rosi, N.; Vodak, D.; Wachter, J.; O'Keefe, M.; Yaghi, O. M. Systematic Design of Pore Size and Functionality in Isoreticular MOFs and Their Application in Methane Storage. *Science* **2002**, *295*, 469–472.
21. Janiak, C. Engineering Coordination Polymers towards Applications. *Dalton Trans.* **2003**, 2781–2804.
22. Mueller, U.; Schubert, M.; Teich, F.; Puetter, H.; Schierle-Arndt, K.; Pastre, J. Metal−Organic Frameworks: Prospective Industrial Applications. *J. Mater. Chem.* **2006**, *16*, 626–636.
23. Kitagawa, S.; Matsuda, R. Chemistry of Coordination Space of Porous Coordination Polymers. *Coord. Chem. Rev.* **2007**, *251*, 2490–2509.
24. Long, J. R.; Yaghi, O. M. The Pervasive Chemistry of Metal−Organic Frameworks. *Chem. Soc. Rev.* **2009**, *38*, 1213–1214.
25. Huang, L. M.; Wang, H. T.; Chen, J. X.; Wang, Z. B.; Sun, J. Y.; Zhao, D. Y.; Yan, Y. S. Synthesis, Morphology Control, and Properties of Porous Metal−Organic Coordination Polymers. *Microporous Mesoporous Mater.* **2003**, *58*, 105–114.
26. Greathouse, J. A.; Allendorf, M. D. The Interaction of Water with MOF-5. *J. Am. Chem. Soc.* **2006**, *128*, 10678.
27. Kondo, A.; Daimaru, T.; Noguchi, H.; Ohba, T.; Kaneko, K.; Kanoh, H. Adsorption of Water on Three-Dimensional Pillared-Layer Metal Organic Frameworks. *J. Colloid Interface Sci.* **2007**, *314*, 422.
28. Henninger, S. K.; Habib, H. A.; Janiak, C. MOFs as Adsorbents for Low Temperature Heating and Cooling Applications. *J. Am. Chem. Soc.* **2009**, *131*, 2776−2777.
29. Castillo, J. M.; Vlugt, T. J. H.; Calero, S. Understanding Water Adsorption in Cu-BTC Metal−Organic Frameworks. *J. Phys. Chem. C* **2008**, *112*, 15934–15939.
30. Küsgens, P.; Rose, M.; Senkovska, I.; Frode, H.; Henschel, A.; Siegle, S.; Kaskel, S. Characterization of Metal−Organic Frameworks by Water Adsorption. *Microporous Mesoporous Mater.* **2009**, *120*, 325.
31. Liu, Y. L.; Kravtsov, V. C.; Larsen, R.; Eddaoudi, M. Molecular Building Blocks Approach to the Assembly of Zeolite-like Metal−Organic Frameworks (ZMOFs) with Extra-Large Cavities. *Chem. Commun.* **2006**, *14*, 1488–1490.
32. Sava, D. F.; Kravtsov, V. C.; Nouar, F.; Wojtas, L.; Eubank, J. F.; Eddaoudi, M. Quest for Zeolite-like Metal−Organic Frameworks: On Pyrimidinecarboxylate Bis-Chelating Bridging Ligands. *J. Am. Chem. Soc.* **2008**, *130*, 3768–3770.
33. Nouar, F.; Eckert, J.; Eubank, J. F.; Forester, T. R.; Eddaoudi, M. Zeolite-like Metal−Organic Frameworks (ZMOFs) as Hydrogen Storage Platform: Lithium and Magnesium Ion-Exchange and H_2-(rho-ZMOF) Interaction Studies. *J. Am. Chem. Soc.* **2009**, *131*, 2864–2870.
34. Babarao, R.; Jiang, J. W. Unprecedentedly High Selective Adsorption of Gas Mixtures in rho Zeolite-like Metal−Organic Framework: A Molecular Simulation Study. *J. Am. Chem. Soc.* **2009**, *131*, 11417–11425.
35. Lee, Y.; Reisner, B. A.; Hanson, J. C.; Jones, G. A.; Parise, J. B.; Corbin, D. R.; Toby, B. H.; Freitag, A.; Larese, J. Z. New Insight into Cation Relocations within the Pores of Zeolite rho: *In Situ* Synchrotron X-ray and Neutron Powder Diffraction Studies of Pb- and Cd-Exchanged rho. *J. Phys. Chem. B* **2001**, *105*, 7188–7199.
36. Shirono, K.; Endo, A.; Daiguji, H. Molecular Dynamics Study of Hydrated Faujasite-Type Zeolites. *J. Phys. Chem. B* **2005**, *109*, 3446–3453.
37. Koneshan, S.; Rasaiah, J. C. Computer Simulation Studies of Aqueous Sodium Chloride Solutions at 298 and 683 K. *J. Chem. Phys.* **2000**, *113*, 8125–8137.
38. Dzhigit, O. M.; Kiselev, A. V.; Mikos, K. N.; Muttik, G. G.; Rahmanova, T. A. Heats of Adsorption of Water Vapour on X-Zeolites Containing Li^+, Na^+, K^+, Rb^+ and Cs^+ Cations. *J. Chem. Soc., Faraday Trans. 1* **1971**, *67*, 458.
39. Bolis, V.; Busco, C.; Ugliengo, P. Thermodynamic Study of Water Adsorption in High-Silica Zeolites. *J. Phys. Chem. B* **2006**, *110*, 14849–14859.

40. Plant, D. F.; Maurin, G.; Deroche, I.; Gaberova, L.; Llewellyn, P. L. CO_2 Adsorption in Alkali Cation Exchanged Y Faujasites: A Quantum Chemical Study Compared to Experiments. *Chem. Phys. Lett.* **2006**, *426*, 387–392.
41. Dang, L. X.; Pettitt, B. M. Simple Intramoleculsr Model Potentials for Water. *J. Phys. Chem.* **1987**, *91*, 3349.
42. Leherte, L.; Andre, J. M.; Derouane, E. G.; Vercauteren, D. P. What Does Zeolitic Water Look Like? Modelization by Molecular-Dynamics Simulations. *Int. J. Quantum Chem.* **1992**, *42*, 1291–1326.
43. Praprotnik, M.; Janezic, D.; Mavri, J. Temperature Dependence of Water Vibrational Spectrum: A Molecular Dynamics Simulation Study. *J. Phys. Chem. A* **2004**, *108*, 11056–11062.
44. Sonoda, M. T.; Moreira, N. H.; Martinez, L.; Favero, F. W.; Vechi, S. M.; Martins, L. R.; Skaf, M. S. A Review on the Dynamics of Water. *Braz. J. Phys.* **2004**, *34*, 3–16.
45. Crupi, V.; Longo, F.; Majolino, D.; Venuti, V. Vibrational Properties of Water Molecules Adsorbed in Different Zeolitic Framework. *J. Phys.: Condens. Matter* **2006**, *18*, 3563–3580.
46. Wu, Y. J.; Tepper, H. L.; Voth, G. A. Flexible Simple Point-Charge Water Model with Improved Liquid-State Properties. *J. Chem. Phys.* **2006**, *124*, 024503-1−024503-12.
47. Frisch, M. J.; Trucks, G. W.; Schlegel, H. B.; Scuseria, G. E.; Robb, M. A.; Cheeseman, J. R.; Zakrzewski, V. G.; Montgomery, J. A.; Stratmann, R. E.; Burant, J. C.; *et al. Gaussian 03*, revision D.01; Gaussian, Inc.: Wallingford, CT, 2004.
48. Rappe, A. K.; Casewit, C. J.; Colwell, K. S.; Goddard, W. A., III.; Skiff, W. M. UFF, a Full Periodic Table Force Field for Molecular Mechanics and Molecular Dynamics Simulations. *J. Am. Chem. Soc.* **1992**, *114*, 10024.
49. Smith, W.; Forester, T. R. Dl_Poly 2.0: A General-Purpose Parallel Molecular Dynamics Simulation Package. *J. Mol. Graphics* **1996**, *14*, 136–141.